Research Square

Preprints are preliminary reports that have not undergone peer review.
They should not be considered conclusive, used to inform clinical practice,
or referenced by the media as validated information.

Detailed Investigation of the Spectroscopic Features of Nicardipine Hydrochloride Using Experimental and Quantum Chemical Methods

Sumeyra Can

sumeyrasacakli@bayburt.edu.tr

Bayburt University

Mehmet Cinar

Technical Scientific Vocational School, Bayburt University

Özlem Baris

Atatürk University

Research Article

Keywords: Calcium channel blockers, DFT, Nicardipine, B3LYP

Posted Date: September 16th, 2025

DOI: https://doi.org/10.21203/rs.3.rs-7546987/v1

License: This work is licensed under a Creative Commons Attribution 4.0 International License. Read Full License

Additional Declarations: No competing interests reported.

Version of Record: A version of this preprint was published at Journal of Molecular Modeling on October 28th, 2025. See the published version at https://doi.org/10.1007/s00894-025-06539-w.

Abstract

Context

The structural and spectroscopic properties of drug groups can be determined using spectroscopic techniques and quantum chemical calculations. In this study, the structural and spectroscopic properties of Nicardipine, a potent calcium channel blocker belonging to the dihydropyridine drug group, were investigated. For this purpose, FT-IR, Raman, NMR and UV-Vis spectra of nicardipine hydrochloride were recorded. The ground state geometry optimisation performed under vacuum conditions showed excellent agreement with X-ray diffraction (XRD) data, with root-mean-square deviations of bond lengths and bond angles calculated as 0.017 Å and 2.2°, respectively. Vibrational spectrum analysis revealed all characteristic modes, and theoretical B3LYP predictions largely agreed with experimental data. NMR spectra recorded in chloroform solvent confirmed the molecular structure of Nicardipine. A comparison with previously reported data revealed significant differences in the proton NMR results, while the carbon NMR data showed consistency. The GIAO method, commonly used for NMR spectrum prediction, yielded results within an acceptable error range despite minor inconsistencies arising from differences between experimental and computational conditions. In the UV-Vis spectrum of Nicardipine HCl, an absorption peak corresponding to π-π* excitation was observed at 238 nm.

Method

The geometric optimisations and vibration spectra of the nicardipine drug molecule were performed using the Gaussian 09 programme with the B3LYP functional and the 6-311 + + G(d,p) basis set. Visualisations were performed using the GaussView 5.0 interface programme. NMR spectra were recorded in chloroform solvent using the GIAO method. Molecular electrostatic potential (MEP) maps and Mulliken atomic charges were analysed to gain deeper insight into the electronic properties.

1. Introduction

The history of calcium channel blockers (CCBs) dates back to the mid-20th century. Preclinical and clinical studies of these drugs and their use in modern medicine for the treatment of various cardiovascular diseases, such as hypertension, angina and some arrhythmias, reflect an important period. The development of CCBs gained momentum in the 1960s when scientists began to investigate coronary dilators [1]. The findings from experimental studies revealing that certain compounds can block the entry of calcium into the cell have led to the inclusion of CCBs in new research [2]. Although several types of these CCBs have been identified, the primary mechanism of action of existing CCBs is to block L-type calcium channels in cardiac and smooth muscle cells. They were first used as first-line pharmaceutical agents in the treatment of hypertension. However, today they are frequently used in the treatment of different health problems such as Raynaud's phenomenon, angina pectoris, migraine and postoperative care [3]. Although regulation of calcium intake is the basis of their therapeutic effects, the physiologic and pathologic implications of these effects are still under investigation. However, since the use of these drugs may be associated with different side effects, controlled monitoring of patients and treatment strategy increases the importance. Experimental studies on the cardiovascular and nervous systems continue to reveal the effects of CCBs day by day.

CCBs are classified into three different categories according to their chemical and pharmacological structures: dihydropyridines, phenylalkylamines and benzothiazepines. Dihydropyridines, whose effects on peripheral arterial smooth muscles are widely known, act as vasodilators that reduce systemic vascular resistance and blood pressure. Nicardipine, a derivative of 1,4-dihydropyridine, is a dihydropyridine calcium channel blocker commonly used in acute and chronic hypertension. The mechanism of action of this drug is to rapidly lower blood pressure by dilating cerebral and coronary blood vessels [4, 5]. Different experimental studies have reported that nicardipine shows antihypertensive activity in hypertensive crises observed in pediatric patients [6] and can be used for neuroprotection in acute neurological cases [7].

When previous studies on Nicardipine HCl were examined, the crystal structures of Nicardipine HCl polymorphs were determined by single crystal XRD method [8]. However, FT-Raman and FT-infrared spectra of hydrogen bonding patterns of seven calcium channel blockers from the dihydropyridine group, including nicardipine, in crystalline and amorphous phases were obtained and reported that the nicardipine drug molecule in the amorphous state has strong average hydrogen bonding [9]. Proton nuclear magnetic resonance spectroscopy (^{1}H NMR) revealed that nicardipine HCl is a molecule with electron-donating groups capable of forming hydrogen bonds [10]. On the other hand, the plasma concentration of nicardipine HCl was determined by reverse-phase liquid chromatography, and it was concluded that the drug has a short half-life [11]. In this study, the ground-state geometrical structure and spectroscopic properties of nicardipine were calculated theoretically by DFT method and re-examined experimentally by IR, Raman, NMR and UV-Vis techniques. Computational and experimental results were comparatively discussed and checked with available data in the literature.

2. Experimental

Nicardipine Hydrochloride was purchased from Apollo Scientific, and used without further purification. Fourier Transform Infrared (FT-IR) spectrum was recorded using a Perkin-Elmer Spectrum One FT-IR spectrometer in the range of 4000 – 400 cm^{-1} at room temperature. Raman spectrum of Nd:

YVO_4 excited with 532 nm laser in the 4000-0 cm^{-1} region Using a Thermo Scientific DXR Raman Microscope with DPSS Raman Spectrophotometer received. Proton (^1H), carbon (^{13}C) and DEPT NMR were obtained in a chloroform solution using a Bruker AVANCE III 400 MHz NMR spectrometer at 19–21°C with tetramethylsilane (TMS) as a reference. UV-Vis measurement was performed using PG INSTRUMENT T80 + spectrophotometer in the wavelength range of 190–400 nm and in distilled water.

3. Quantum Chemical Calculations

All calculations to assess the structural and spectroscopic properties were conducted using the Gaussian 09 software package [12, 13], employing Density Functional Theory (DFT) with the B3LYP functional and the 6-311 + + G(d,p) basis set [14–18]. The initial step of the calculations involves determining the optimal geometric structure of the isolated Nicardipine molecule in a vacuum. Once the ground-state geometric structure was established, it was utilized as input structure to interpret vibrational spectra, chemical shifts, and electronic properties. From the vibrational calculations, the reduced mass, force constant, IR absorption intensity, and Raman scattering activities associated with each vibrational frequency were determined for the studied compound. In vibrational analysis, neglecting electron correlation and system errors from an inadequate basis set can result in an overestimation of vibrational wavenumbers. To address the discrepancies between the recorded vibrational modes and those calculated, one can apply a scaled field, explicitly calculate anharmonic corrections, or multiply the wavenumbers obtained from quantum chemical calculations by an appropriate scaling coefficient [19]. Moreover, one reason for the difference between the values obtained from experimental and quantum chemical calculations is that the vibrational modes are theoretically derived for an isolated molecule in the gas phase, unaffected by external factors like Coulomb interactions. In contrast, experimental studies generally involve molecules in the solid phase. In this study, two scaling factors were applied: 0.983 for the 0-1700 cm^{-1} range and 0.958 for the 1700–4000 cm^{-1} range, in order to align the predicted values more closely with the observed peaks [20–22]. The chemical shift values of the compound were calculated in the gas phase, as well as in chloroform and DMSO (dimethyl sulfoxide) solutions, using the Gauge-Invariant Atomic Orbital (GIAO) method [23, 24], with TMS as the reference standard [25–27]. The electronic properties of the molecule were assessed using the TD-DFT [28–31] method in the gas phase, as well as in ethanol, methanol, and THF (tetrahydrofuran) solvents. The HOMO-LUMO energy gap, dipole moment, oscillator strengths, and absorption wavelengths for the first three excited states were evaluated. Molecular Electrostatic Potential (MEPS) [32–34] was also utilized to analyze intermolecular interactions and identify nucleophilic and electrophilic binding sites within the system.

Electrostatic Potential (MESP) [35–37] and Mulliken Charge Analysis [38] were also used to describe inter-molecular interactions and determine the electrical properties.

4. Results and Discussion

4.1. Molecular Geometry

The molecular structure of nicardipine hydrochloride was elucidated through single crystal X-ray diffraction analysis, as detailed in the study conducted by Moreno-Calvo et al. [8]. The ground-state geometric structure of the Nicardipine molecule, excluding the hydrochloride component, was determined using DFT calculations, and is presented in Fig. 1 (and Figs. S1).

In Table 1, the computed geometrical parameters such as bond lengths and bond angles are presented with comparison of the experimentally obtained data reported in literature [8]. It's important to note that the experimental values were derived from single crystal X-ray diffraction in the solid phase, while the geometrical optimization for the isolated molecules was conducted in a vacuum and without considering the hydrochloride component. Therefore, some discrepancies between the experimental and theoretical results are anticipated.

Table 1
The comparison of the computed and observed geometrical parameters of Nicardipine. Bond lengths in Angstrom (Å) and bond angles in degrees (°).

Bond Lengths	B3LYP	Exp.[8]	Bond Lengths	B3LYP	Exp.[8]	Bond Angles	B3LYP	Exp.[8]	Bond Angles	B3LYP	Exp.[1]	Bond Angles	B3LYP	Exp.[8]
O(1)-C(16)	1,357	1,354	C(33)-C(35)	1,392	1.352	C(16)-O(1)-C(23)	118,0	118,9	C(17)-C(24)-C(27)	122,3	122,9	H(43)-C(21)-H(45)	108,5	-
O(1)-C(23)	1,442	1,433	C(34)-C(35)	1,396	1.372	C(20)-O(2)-C(32)	115,7	116,3	C(18)-C(25)-C(27)	120,5	120,8	H(44)-C(21)-H(45)	106,4	-
O(2)-C(20)	1,359	1,354	N(8)-C(29)	1,459	1.485	C(14)-N(7)-C(15)	124,2	123,5	N(8)-C(26)-C(28)	113,6	112,0	N(8)-C(22)-H(46)	111,5	-
O(2)-C(32)	1,436	1,442	C(10)-H(36)	1,088	-	C(14)-N(7)-H(37)	116,9	119,1	C(24)-C(27)-C(25)	117,8	117,7	N(8)-C(22)-H(47)	108,2	-
O(3) = C(16)	1,216	1,205	C(17)-H(38)	1,081	-	C(15)-N(7)-H(37)	116,9	116,5	C(26)-C(28)-C(30)	121,2	120,2	C(23)-C(22)-H(46)	107,3	-
O(4) = C(20)	1,216	1,202	C(18)-H(29)	1,083	-	C(11)-C(10)-C(12)	111,0	111,2	C(26)-C(28)-C(31)	120,0	120,9	C(23)-C(22)-H(47)	108,0	-
O(5)-N(9)	1,224	1,225	C(19)-H(40)	1,088	-	C(11)-C(10)-C(13)	110,9	112,1	C(30)-C(28)-C(31)	118,6	118,8	H(46)-C(22)-H(47)	106,9	-
O(6) = N(9)	1,228	1,221	C(19)-H(41)	1,091	-	C(12)-C(10)-C(13)	111,9	110,2	C(28)-C(30)-C(33)	120,8	120,2	O(1)-C(23)-H(48)	109,1	-
N(7)-C(14)	1,388	1,368	C(19)-H(42)	1,093	-	C(10)-C(11) = C(14)	120,3	120,8	C(28)-C(31)-C(34)	120,8	120,2	O(1)-C(23)-H(49)	105,5	-
N(7)-C(15)	1,385	1,376	C(21)-H(43)	1,093	-	C(10)-C(11)-C(16)	114,2	118,0	C(30)-C(33)-C(35)	120,0	120,6	C(22)-C(23)-H(48)	112,8	-
N(7)-H(37)	1,007	0,880	C(21)-H(44)	1,088	-	C(14) = C(11)-C(16)	125,3	121,2	C(31)-C(34)-C(35)	120,0	120,1	C(22)-C(23)-H(49)	109,0	-
N(8)-C(22)	1,458	1,489	C(21)-H(45)	1,092	-	C(10)-C(12) = C(15)	120,2	121,4	C(33)-C(35)-C(34)	119,6	120,0	H(48)-C(23)-H(49)	108,9	-
N(8)-C(26)	1,467	1,513	C(22)-H(46)	1,109	-	C(10)-C(12)-C(20)	119,5	117,6	C(22)-N(8)-C(26)	111,7	-	C(18) = C(25)-H(50)	119,9	-
N(9)-C(24)	1,477	1,468	C(22)-H(47)	1,092	-	C(15) = C(12)-C(20)	120,1	120,9	C(22)-N(8)-C(29)	112,6	-	C(27)-C(25)-H(50)	119,5	-
C(10)-C(11)	1,527	1,525	C(23)-H(48)	1,088	-	C(10)-C(13)-C(17)	120,6	120,9	C(26)-N(8)-C(29)	111,7	-	N(8)-C(26)-H(51)	111,6	-
C(10)-C(12)	1,525	1,523	C(23)-H(49)	1,092	-	C(10)-C(13)-C(18)	120,9	120,8	O(5)-N(9) = O(6)	124,2	-	N(8)-C(26)-H(52)	107,0	-
C(10)-C(13)	1,533	1,528	C(25)-H(50)	1,083	-	C(17)-C(13)-C(18)	118,4	118,4	O(5)-N(9)-C(24)	117,9	-	C(28)-C(26)-H(51)	109,3	-
C(11) = C(14)	1,359	1,353	C(26)-H(51)	1,105	-	N(7)-C(14)	118,3	120,4	O(6) = N(9)-C(24)	117,8	-	C(28)-C(26)-H(52)	108,5	-

Bond Lengths	B3LYP	Exp.[8]	Bond Lengths	B3LYP	Exp.[8]	Bond Angles	B3LYP	Exp.[8]	Bond Angles	B3LYP	Exp.[1]	Bond Angles	B3LYP	Exp.[8]
						= C(11)								
C(11)-C(16)	1,472	1,463	C(26)-H(52)	1,094	-	N(7)-C(14)-C(19)	113,4	114,0	C(11)-C(10)-H(36)	107,5	-	H(51)-C(26)-H(52)	106,3	-
C(12) = C(15)	1,359	1,351	C(27)-H(53)	1,081	-	C(11) = C(14)-C(19)	128,2	125,6	C(12)-C(10)-H(36)	108,7	-	C(24) = C(27)-H(53)	120,0	-
C(12)-C(20)	1,470	1,461	C(29)-H(54)	1,090	-	N(7)-C(15) = C(12)	118,5	119,6	C(13)-C(10)-H(36)	106,4	-	C(25)-C(27)-H(53)	122,1	-
C(13)-C(17)	1,395	1,382	C(29)-H(55)	1,106	-	N(7)-C(15)-C(21)	114,3	113,3	C(13) = C(17)-H(38)	121,4	-	N(8)-C(29)-H(54)	110,2	-
C(13)-C(18)	1,398	1,392	C(29)-H(56)	1,091	-	C(12) = C(15)-C(21)	127,0	127,1	C(24)-C(17)-H(38)	118,9	-	N(8)-C(29)-H(55)	112,6	-
C(14)-C(19)	1,506	1,505	C(30)-H(57)	1,085	-	O(1)-C(16) = O(3)	122,8	121,3	C(13)-C(18)-H(39)	118,9	-	N(8)-C(29)-H(56)	109,4	-
C(15)-C(21)	1,504	1,503	C(31)-H(58)	1,084	-	O(1)-C(16)-C(11)	114,2	109,6	C(25) = C(18)-H(39)	119,8	-	**r.m.s.**	**2,2**	
C(17)-C(24)	1,389	1,383	C(32)-H(59)	1,088	-	O(3) = C(16)-C(11)	122,8	129,1	C(14)-C(19)-H(40)	111,2	-			
C(18)-C(25)	1,395	1,382	C(32)-H(60)	1,091	-	C(13)-C(17)-C(24)	119,6	119,3	C(14)-C(19)-H(41)	110,9	-			
C(22)-C(23)	1,524	1,511	C(32)-H(61)	1,091	-	C(13)-C(18)-C(25)	121,2	120,9	C(14)-C(19)-H(42)	110,3	-			
C(24)-C(27)	1,392	1,366	C(33)-H(62)	1,084	-	O(2)-C(20) = O(4)	121,7	120,5	H(40)-C(19)-H(41)	107,3	-			
C(25)-C(27)	1,390	1,378	C(34)-H(63)	1,084	-	O(2)-C(20)-C(12)	111,5	111,2	H(40)-C(19)-H(42)	108,5	-			
C(26)-C(28)	1,516	1,502	C(35)-H(64)	1,084	-	O(4) = C(20)-C(12)	126,6	128,3	H(41)-C(19)-H(42)	108,3	-			
C(28)-C(30)	1,396	1,383	**r.m.s.**	**0,017**		N(8)-C(22)-C(23)	114,4	113,9	C(15)-C(21)-H(43)	110,4	-			
C(28)-C(31)	1,400	1,378				O(1)-C(23)-C(22)	110,8	101,5	C(15)-C(21)-H(44)	111,3	-			
C(30)-C(33)	1,396	1,380				N(9)-C(24)-C(17)	118.6	118,0	C(15)-C(21)-H(45)	110.7	-			
C(31)-C(34)	1,392	1,383				N(9)-C(24)-C(27)	119,0	119,1	H(43)-C(21)-H(44)	109,2	-			

According to root mean square (r.m.s.) calculations, the predicted bond lengths and angles were highly accurate, differing by only 0.017 Å and 2.20 degrees, respectively. Analyzing the bond lengths, it is observed that DFT calculations indicate the three carbon bonds attached to the N(8) atom and the bond between O(2) and the methyl group to be longer than the experimental values. In contrast, for all other bond lengths, DFT results were

either consistent with the experimental measurements or slightly shorter. The absence of HCl in the calculations can be considered the most significant factor in the differing predictions of the carbon bonds with N(8). The crystallographic structure indicates that HCl is positioned close to this atom. Due to the electronic interactions between these atoms, the bond lengths are found to be greater than their actual values. Additionally, the crystallographic structure suggests that interactions may occur between the phenyl ring, which lacks any functional groups within the unit cell, and the pyridine ring of the other molecule. Therefore, the C-C bonds in the phenyl ring and the N-C bond in the pyridine ring have been predicted to show the most deviation from the experimental values. The most significant difference in bond angles was observed for the O(1)-C(23)-C(22) bond, which exhibited a deviation of 9.30 degrees. The C(16)-C(11)-O(1) bond angle was calculated to be larger than expected, with an error of 4.60 degrees, while the C(16)-C(11)-O(3) bond angle was found to be smaller, with an error of 6.30 degrees. The relationship equations and R^2 values obtained from the linear correlation between measured and predicted values are given in Fig. S2.

4.2. Vibrational Analysis

This section provides an analysis of the recorded and calculated vibrational spectra (IR and Raman), highlighting key vibrational modes and their significance. The experimentally recorded FT-IR and Raman spectra of Nicardipine hydrochloride are presented in Fig. 2 while the resulting spectra for the vibrational modes quantum chemical calculations are displayed in Fig. 3.

The data obtained from the vibrational calculations, including vibrational wavelengths, reduced mass, force constants, IR intensities, and Raman activities, along with the values of the recorded vibrational peaks, are summarized in Table S1.

Although O–H, N–H, and C–H stretching absorption bands are confined to a narrow region above 3000 cm^{-1}, they provide crucial insights into molecular structure. For compounds containing one or more aromatic rings, as in this study, C–H and C = C–C vibrations are key indicators. C–H stretching in aromatic rings is usually found in the 3000–3100 cm^{-1} range with low absorption intensities, though some overtone and combination effects may also place vibrations below 3000 cm^{-1}. Above 3000 cm^{-1}, carbon and hydrogen atoms move radially in opposite directions, while vibrations below this threshold involve them moving in the same direction with minimal bond length change. Aliphatic C–H stretching vibrations are typically recorded below 3000 cm^{-1}.

The C-H stretching vibrations of the aromatic rings in Nicardipine HCl were recorded in the range of 3027–3180 cm^{-1} and identified as pure vibrations. In contrast, the C-H stretching modes from aliphatic hydrocarbons and methyl groups within the compound's structure were observed and calculated to occur in the region 2937–2993 cm^{-1} slighly below 3000 cm^{-1}. The N-H stretching peak was observed at approximately 3250 cm^{-1} in the FT-IR spectrum. C = C-C stretching is another characteristic vibrational mode that indicates the presence of aromatic rings in a structure, typically observed in the 1400–1650 cm^{-1} region.

The peaks recorded at 1620 cm^{-1} in FT-IR analysis and 1583 cm^{-1} in Raman spectrum were calculated with high accuracy using DFT and identified as pure C = C-C stretching vibrations of aromatic rings. The peaks observed at 1703 and 1645 cm^{-1} (1706 and 1643 cm^{-1} in Raman spectrum) in the FT-IR analysis are characteristic of C = O stretching vibrations, and they are clearly and strongly represented in both methods. The vibrational mode observed at 1533 cm^{-1} in the FT-IR and at 1527 cm^{-1} in the Raman spectrum, with a DFT estimate of 1548 cm^{-1}, indicates the presence of NO_2 in the structure of Nicardipine HCl and is assigned as an asymmetric N-O vibration.

In aromatic compounds, C-H in-plane bending vibrations are typically observed in the range of 1000–1300 cm^{-1}, while out-of-plane vibrations occur in the region of 700–1000 cm^{-1}. Additionally, C-H in-plane bending vibrations that are not part of a ring can be detected up to 1500 cm^{-1}, resulting in some overlap within this region. The C-H in-plane bending vibrations of Nicardipine HCl, including those associated with the aromatic rings, were observed over a broad range of 1000–1500 cm^{-1}. The bending vibrations of the aromatic ring are significantly contaminated with the C-C stretching vibrations of the ring. Aromatic ring C-H and CCCC out-of-plane bending vibrations were calculated and recorded in the region specified in the literature. While these vibrations were occasionally contaminated with other out-of-plane C-H bendings, they were generally observed as pure vibrations. The peak recorded at 943 cm^{-1} in the FT-IR spectrum was assigned as the O-CH_3 stretching of the acetyl group. In addition, the N-H out-of-plane bending vibration was calculated to be 491 cm^{-1}.

4.3. Nuclear Magnetic Resonance (NMR) Analysis

The experimental proton (^1H), carbon (^{13}C), and DEPT NMR chemical shift values of Nicardipine HCl were recorded in chloroform ($CDCl_3$) as the solvent. NMR properties, which are crucial for determining molecular structure, are also commonly utilized in computational studies because they offer insights into the electronic origins of nuclear shielding and the variations in its magnitude. Hence, the chemical shifts of the molecules were calculated in the gas phase as well as in chloroform and DMSO (dimethyl sulfoxide) solvents using the GIAO (Gauge Invariant Atomic Orbital) method, which is a standard approach for calculating NMR spectra. In both theoretical and experimental studies, tetramethylsilane (TMS) was used as a reference substance due to its notable advantages, including inertness, a signal in various solvents, and a low boiling point of 27°C. The recorded and computed chemical shift values are presented comparatively in Table 2. This table also includes previously published experimental data [11]. While the ^{13}C NMR values align well with those recorded in this study, there is a significant discrepancy observed in the ^1H NMR data. The ^1H and ^{13}C NMR spectra recorded for Nicardipine HCl are given in Figs. 4a and 4b respectively, while the DEPT NMR spectrum of this compound is shown in Fig. S3. The peak observed at 11.25 ppm corresponds to the hydrogen atom bonded to nitrogen, with its resonance shifting downfield due to factors such as intermolecular interactions and solvent-solute effects. As a result, the DFT calculation yielded a value that is considerably

different. It has been reported in the literature that the peak at 7.20 ppm corresponds to the same hydrogen [11]. The CH_3 protons in the acetyl group resonated at 3.56 ppm. In contrast, the methyl group attached to nitrogen exhibited three different values at 2.51, 2.56, and 2.58 ppm, with relatively small shifts for each hydrogen. As expected, the presence of electron-withdrawing atoms like oxygen and nitrogen caused the chemical resonances of these methyl groups to appear in the downfield region. The chemical shift values obtained for the methyl groups attached to the pyrimidine ring are 2.35 and 2.29 ppm. A slight difference in the resonances of these atoms was observed, attributed to their neighboring chemical environments. The hydrogens belonging to the aliphatic group were observed to resonate at 4.19 ppm for H(46) and 4.32 ppm for H(47). Although both hydrogens are bonded to the C(22) carbon atom, the bond angles they form with this carbon and the nitrogen atom differ by approximately 30 degrees. This difference in geometry resulted in distinct chemical shifts for each hydrogen. In addition, both hydrogens H(48) and H(49) produced peaks at 4.43 ppm, while hydrogens H(51) and H(52) resonated at 3.40 ppm. The chemical shift for H(36), which is attached to the C(10) carbon in the pyrimidine ring, was recorded at 5.00 ppm. Hydrogens in the aromatic rings resonated in the range of 7.44–7.97 ppm, with H(38) and H(53) exhibiting lower chemical shifts at 7.97 and 7.95 ppm, respectively, due to the influence of the NO_2 group.

Table 2
The recorded and predicted 13C and 1H NMR isotropic chemical shifts (with respect to TMS, all values in ppm) for Nikardipine (HCl).

	Experimental		B3LYP/6-311 + + G(d,p)				Experimental		B3LYP/6-311 + + G(d,p)		
Atom	This study	Ref. [11]	Gas	DMSO	Chloroform	Atom	This study	Ref. [11]	Gas	DMSO	Chloroform
C(20)	167,45	167,48/167,45	176,2	178,2	177,6	H(38)	7,97	8,05/8,04	9,54	9,60	9,57
C(16)	166,52	166,29/166,24	175,8	178,0	177,3	H(53)	7,95	7,94/7,89	8,96	9,06	9,02
C(13)	150,08	149,42/149,39	163,2	164,2	164,0	H(39)	7,51	7,61	8,79	8,87	8,86
C(24)	148,67	148,49	160,2	161,7	161,2	H(63)	7,58	7,43	8,28	8,23	8,23
C(15)	146,86	145,53	156,6	160,7	159,4	H(64)	7,48	7,41	8,10	8,22	8,18
C(14)	148,16	148,10	154,2	158,7	157,2	H(50)	7,63	7,36/7,31	8,10	8,35	8,27
C(28)	129,20	128,03/128,00	150,7	152,7	152,1	H(62)	7,61	7,43	8,01	8,18	8,12
C(18)	134,40	134,13/134,09	146,1	147,2	147,1	H(57)	7,44	7,55	7,85	8,07	7,99
C(31)	131,67	131,07/131,04	140,0	140,3	140,4	H(58)	7,44	7,55	7,48	7,50	7,51
C(34)	130,46	129,43	138,3	138,4	138,2	H(48)	4,43	4,63	6,13	6,07	6,09
C(30)	131,67	131,07/131,04	138,0	139,6	139,0	H(36)	5,00	5,06/5,05	5,99	5,91	5,94
C(35)	130,13	130,33	136,1	136,4	136,2	H(37)	11,25	7,20	5,55	6,37	6,10
C(33)	130,46	129,43	136,0	137,1	136,6	H(61)	3,56	3,65/3,64	4,40	4,41	4,41
C(25)	129,91	129,18/129,11	134,6	136,5	136,0	H(60)	3,56	3,65/3,64	4,23	4,22	4,23
C(17)	121,95	122,36	133,7	134,8	134,4	H(59)	3,55	3,65/3,64	4,20	4,41	4,35
C(27)	121,69	121,40	130,4	131,6	131,2	H(52)	3,40	4,06/3,95	4,09	4,13	4,13
C(11)	100,18	100,52/100,44	116,8	115,8	116,2	H(49)	4,43	4,62	3,91	4,13	4,06
C(12)	101,73	103,01	113,7	113,0	113,2	H(54)	2,58	2,66/2,57	3,87	3,75	3,80
C(26)	59,00	60,52/60,26	70,8	70,5	70,6	H(44)	2,29	2,38	3,67	3,44	3,52
C(23)	58,58	57,96/57,88	65,0	66,0	65,7	H(51)	3,40	4,21	3,50	3,69	3,61
C(22)	53,66	54,20/54,03	61,8	62,1	62,0	H(47)	4,32	3,38	3,37	3,34	3,35
C(32)	51,33	51,16/51,14	56,2	57,0	56,7	H(45)	2,29	2,38	3,21	3,12	3,16
C(10)	39,13	39,33	50,0	50,7	50,5	H(41)	2,35	2,42/2,41	3,17	3,18	3,17
C(29)	39,99	40,00/39,76	47,0	47,2	47,2	H(40)	2,35	2,42/2,41	2,95	2,72	2,80
C(19)	18,99	19,58	28,4	28,8	28,6	H(56)	2,56	2,66/2,57	2,72	2,78	2,77
C(21)	18,69	19,28	26,6	27,0	26,8	H(55)	2,51	2,66/2,57	2,31	2,46	2,39
						H(46)	4,19	3,18	2,30	2,52	2,43
						H(43)	2,29	2,38	1,67	2,14	1,99
						H(42)	2,35	2,42/2,41	1,39	1,83	1,68

Atomic numbering was done according to Fig. 1.

Examining the ^{13}C NMR data, the peaks in the highest region, at 18.69 and 18.99 ppm, correspond to the C(21) and C(19) atoms of the methyl groups attached to the pyrimidine ring, respectively. The chemical shift values for methyl groups attached to nitrogen and oxygen atoms were observed as 39.99 and 51.33 ppm, respectively. The C(20) atom, which is bonded to two electronegative oxygen atoms, loses electrons and resonates in the lowest region of the spectrum at 167.45 ppm. A similar situation applies to C(16), with its chemical shift value recorded at 166.52 ppm. Aromatic carbon resonances typically occur in the region of 100–150 ppm; however, the exact resonances can vary depending on the substituents attached to the ring. The presence of multiple electron-withdrawing or electron-donating groups can lead to chemical shift values ranging from 90 to 180 ppm. When examining the ring attached to the chain group, it is observed that the aromatic carbons resonate around 130 ppm. Specifically, the C(24) carbon, which is directly bonded to the NO_2 functional group, exhibits a chemical shift at 148.67 ppm. Meanwhile, the chemical shift for C(13), which is attached to the other ring, was recorded at 150.08 ppm. Other carbon atoms resonated at approximately 121, 130, and 134 ppm, depending on their surrounding environment. As anticipated, the chemical shift values of the pyrimidine ring carbons were

significantly influenced by the substituents attached to the ring. For instance, the chemical shift values for the C(14) and C(15) atoms, which have methyl groups attached, were observed at 146.86 and 148.16 ppm, respectively. In contrast, the C(11) and C(12) atoms exhibited chemical shifts around 100 ppm. The chemical shift for C(10), which is directly connected to another aromatic ring, was recorded at 39.13 ppm. The chemical shift values for the C(26), C(23), and C(22) carbons—each bonded to one atom such as oxygen or nitrogen and also connected to two hydrogens and one carbon—were recorded at 59.00, 58.58, and 53.66 ppm, respectively.

Although the calculations for the examined molecule did not exactly match the experimental values, the results were consistent within an acceptable margin of error. It was concluded that the geometrical structure of the molecule could be effectively assessed using both the calculated values and the observed spectra.

4.4. Electronic Properties Analysis

To investigate the electronic transitions of the Nicardipine molecule, we performed Time-Dependent Density Functional Theory (TD-DFT) calculations [31].

These calculations solve the time-dependent Schrödinger equation for systems of atoms and electrons, enabling us to simulate electronic excitations in materials and molecules. Specifically, we analyzed the electronic absorption spectrum by examining the three lowest singlet → singlet spin-allowed excited states in both vacuum and various solvents, including water, ethanol, methanol, and THF. The UV-Vis spectrum of nicardipine HCl in distilled water, as shown in Fig. 5, reveals two absorption peaks at 210 nm and 236 nm. An absorption peak at 238 nm was observed for nicardipine HCl in solvent [11]. Table 3 presents the theoretical absorption wavelengths, excitation energies, and oscillator strengths for the Nicardipine molecule. TD-DFT predicts an electron transition from HOMO to LUMO + 2 at the significant absorption peak of about 355 nm, which exhibits the highest oscillator strength. This transition is assigned as a $\pi \rightarrow \pi^*$ transition. The HOMO and LUMO, along with other significant molecular orbitals where electronic transitions were observed, are depicted in Fig. S4, while the energy values of the molecular orbitals and the electronic absorption energies are summarized in Table S2. The Molecular Electrostatic Potential (MESP) map serves as an essential tool for exploring intermolecular interactions in molecular systems and pinpointing locations for nucleophilic and electrophilic attacks. These maps employ a color gradient from red to dark blue to illustrate regions of strong negativity and positivity within the structure. The order of potential growth is as follows: red < orange < yellow < green < blue. The MESP for nicardipine is illustrated in Fig. 6. Here, the dark blue electronegative region surrounding the N(7) atom indicates its potential role in intermolecular interactions or in the interaction of hydrogen bonded to the nitrogen atom with HCl. On the other hand, the areas around the orange oxygen atoms, which correspond to relatively less negative regions, suggest the possibility of intermolecular bonding in those areas. Mulliken Population Analysis is frequently employed to qualitatively estimate the partial atomic charges of a molecule, as it assesses how the electronic structure varies with atomic displacement. This analysis can provide insights into various molecular properties, including dipole moments, polarizability, and electronic structure. Therefore, the Mulliken atomic charges have been calculated and presented in Table S3.

Table 3
The calculated absorption wavelength, λ (nm), excitation energies E (eV) and oscillator strengths (f) of investigated compounds.

	Ethanol	Gas	Methanol	THF	Water
λ (nm)	496,46	496,46	497,38	487,65	499,12
	458,34	458,34	458,87	452,1	459,76
	354,76	354,76	355,01	354,01	355,51
E (eV)	2,4974 (127 → 128)	2,4974 (127 → 128)	2,4927 (127 → 128)	2,5425 (127 → 128)	2,4841 (127 → 128)
	2,7051 (126 → 128)	2,7051 (126 → 128)	2,7019 (126 → 128)	2,7424 (126 → 128)	2,6967 (126 → 128)
	3,4949 (125 → 128)	3,4949 (125 → 128)	3,4924 (125 → 128)	3,5022 (127 → 129)	3,4875 (125 → 128)
f	0,0001	0,0001	0,0001	0,0001	0,0001
	0,0001	0,0001	0,0001	0,0001	0,0001
	0,0387	0,0387	0,0043	0,1733	0,0016

HOMO and LUMO energy values can be used to calculate the basic properties of a molecular system or molecule: electronegativity, electronic chemical potential, electrophilic index, chemical hardness and softness [39]. In Table S4, all the properties listed above were calculated using the HOMO and LUMO energy values. Nicardipine has an electronegativity of 4.38, a chemical hardness of 1.72 and an electrophilicity index value of 5.58. This molecule exhibits positive A and χ values, suggesting that when electron-nuclear attraction outweighs electron-electron repulsion, it no longer chooses to accept electrons.

5. Conclusion

This study provides a comprehensive spectroscopic characterization of the Nicardipine HCl molecule, employing both experimental techniques (FT-IR, FT-Raman, NMR, and UV-Vis) and quantum chemical methods (DFT and TD-DFT). The results from experimental analyses were compared with computational findings and existing literature data. A critical step in these calculations is determining the ground-state geometrical structure of the molecule. For this purpose, the geometry of Nicardipine was optimized using the B3LYP functional in a vacuum environment and without the HCl adduct. The calculated geometric parameters were compared with experimentally obtained crystallographic data, yielding strong linear correlations. Specifically, the R^2 values for bond lengths and bond angles were found to be 0.996 and 0.982, respectively, while root-mean-square (r.m.s) deviations were 0.017 Å for bond lengths and 2.2° for bond angles. Notable deviations from experimental values were primarily attributed to the influence of electronegative nitrogen atoms. For example, bond lengths and angles involving carbon atoms bonded to N(7) and N(9) were overestimated, while those bonded to N(8) were underestimated. These deviations arise from changes in the electronic distribution around the nitrogen atoms. The vibrational characteristics of Nicardipine were analyzed through FT-IR and Raman spectroscopy, with significant frequencies identified. The B3LYP-calculated vibrational frequencies, scaled with appropriate correction factors, showed good agreement with experimental data. Proton and carbon chemical shifts were analyzed using NMR spectroscopy, a pivotal tool for structural determination. Interestingly, the proton NMR data obtained in this study differed significantly from previously reported values, leading to the addition of corrected results to the literature. NMR chemical shifts predicted using the GIAO method showed discrepancies compared to experimental values due to the vacuum environment used in calculations, the single-molecule model, and minor geometric differences affecting electronic distributions. However, the GIAO method demonstrated internal consistency and provided reliable molecular structure predictions. UV-Vis spectroscopy, being highly sensitive to electronic distributions, exhibited notable differences between experimental and theoretical results. For instance, the experimentally observed absorption peak at 238 nm was predicted at 355 nm using TD-DFT. Such discrepancies emphasize the need for caution when comparing quantum chemical results with experimental UV-Vis data. Finally, the electronic properties of Nicardipine were thoroughly evaluated through molecular orbital analysis, molecular electrostatic potential (MESP) mapping, and Mulliken atomic charge calculations, offering a deeper understanding of its electronic structure. This comprehensive approach bridges experimental and theoretical insights, contributing valuable information to the literature.

Declarations

Ethical Approval

Not applicable.

Funding

No funding was received for this study.

Availability of data and materials

Data will be made applicable on request of reader.

Authorship Contribution Statement

Sümeyra CAN: Review & Editing, Software, Visualization, Conceptualization, Writing, Project administration**,** Original Draft **Mehmet ÇINAR:** Writing, Review & Editing, Software. **Özlem BARIŞ:** Review & Editing, Investigation, Data Curation.

Declaration of Competing Interest

The authors declare that they have no known competing financial interests or personal relationships that could have appeared to influence the work reported in this paper.

Acknowledgments

This work was supported by Atatürk University Research fund through research Grant No: FDK-2022-11079

References

1. Abernethy DR, Schwartz JB (1999) Calcium-antagonist drugs. N Engl J Med 341:1447-1457. http://doi.org/10.1056/NEJM199911043411907
2. Godfraind T (2017) Discovery and development of calcium channel blockers. Front Pharmacol 8:286. http://doi.org/10.3389/fphar.2017.00286
3. Rirash F, Tingey PC, Harding SE, Maxwell LJ, Ghogomu ET, Wells GA, Tugwell P, Pope J (2017) Calcium channel blockers for primary and secondary raynaud's phenomenon. Cochrane Database Syst Rev 12:CD000467. http://doi.org/10.1002/14651858.cd000467.pub2
4. Daou B, Koduri S, Thompson B, Chaudhary N, Pandey A (2019) Clinical and experimental aspects of aneurysmal subarachnoid hemorrhage. CNS Neurosci Ther 25(10):1096-1112. http://doi.org/10.1111/cns.13222
5. Huang BR, Chang PC, Yeh WL, Lee CH, Tsai CF, Lin C, Lin HY, Liu YS, Wu CYJ, Ko PY, Huang SS, Hsu HC, Lu DY (2014) Anti-neuroinflammatory effects of the calcium channel blocker nicardipine on microglial cells: implications for neuroprotection. PloS One 9(3):e91167,

http://doi.org/10.1371/journal.pone.0091167

6. Lee K, Lee I, Park S, Kim J, Oh J, Smith L (2016) Hypertensive crisis in children: an experience in a single tertiary care center in korea. Clin Hypertens 22:10. http://doi.org/10.1186/s40885-016-0040-2
7. Shah Q, Georgiadis A, Suri M, Rodriguez G, Qureshi A (2007) Preliminary experience with intra-arterial nicardipine in patients with acute ischemic stroke. Neurocritical Care 7:53-57, http://doi.org/10.1007/s12028-007-0035-7
8. Moreno-Calvo E, Munto M, Wurst K, Ventosa N, Masciocchi N, Veciana J (2011) Polymorphs and solvates of nicardipine hydrochloride. Selective stabilization of different diastereomeric racemates. Mol Pharmaceutics 8(2):395-404. https://doi.org/10.1021/mp100251s
9. Tang XC, Pikal MJ, Taylor LS (2002) A spectroscopic investigation of hydrogen bond patterns in crystalline and amorphous phases in dihydropyridine calcium channel blockers. Pharm Res 19:477-483. https://doi.org/10.1023/A:1015147729564
10. Fernandes CM, Carvalho RA, da Costa SP, Veiga FJ (2003) Multimodal molecular encapsulation of nicardipine hydrochloride by β-cyclodextrin, hydroxypropyl-β-cyclodextrin and triacetyl-β-cyclodextrin in solution. Structural studies by 1H NMR and ROESY experiments. Eur J Pharm Sci 18:1285-296. https://doi.org/10.1016/S0928-0987(03)00025-3
11. Fernandes CM, Veiga FJB (2003) A simple method for nicardipine hydrochloride quantification in plasma using solid-phase extraction and reversed-phase high- performance liquid chromatography. Biomed Chromatogr 17:33-38. https://doi.org/10.1002/bmc.206
12. Frisch A, Gaussian 09W, Reference. Wallingford, USA, 25:470.
13. Frisch M, Trucks G, Schlegel HB, Scuseria GE, Robb MA, Cheeseman JR, Scalmani G, Barone G, Mennucci B, Petersson G (2009) Gaussian 09, Revision D.01, Gaussian, Inc., Wal-lingford, CT, USA 201.
14. Becke AD (1993b) Density–functional thermochemistry. III. The role of exact exchange. J Chem Phys 98:5648–5652. https://doi.org/10.1007/s002149900065
15. Becke AD (1993a) A new mixing of Hartree–Fock and local density–functional theories. J Chem Phys 98:1372–1377. https://doi.org/10.1063/1.464304
16. Hohenberg P, Kohn W (1964) Inhomogeneous Electron Gas. Phys Rev 136:864-871. https://doi.org/10.1103/PhysRev.136.B864
17. Kohn W, Sham J (1965) Self-Consistent Equations Including Exchange and Correlation Effects. Phys Rev 140:1133-1138. https://doi.org/10.1103/PhysRev.140.A1133
18. Foresman JB, Frisch Æ (1996) Exploring Chemistry with electronic structure methods (2nd ed.) Gaussian Inc., Pittsburgh, PA. ISBN: 9780963676931 303.
19. Scott AP, Radom L (1996) Harmonic vibrational frequencies: an evaluation of Hartree-Fock, Møller-Plesset, quadratic configuration interaction, density functional theory, and semiempirical scale factors. J Phys Chem 100(41):16502-16513. https://doi.org/10.1021/jp960976r
20. Sundaraganesan N, Ilakiamani S, Saleem H, Wojciechowski PM, Michalska D (2005) FT-Raman and FT-IR spectra, vibrational assignments and density functional studies of 5-bromo-2-nitropyridine. Spectrochim Acta A Mol Biomol Spectrosc 61(13-14):2995-3001. https://doi.org/10.1016/j.saa.2004.11.016
21. Sundaraganesan N, Priya M, Meganathan C, Joshua BD, Cornard JP (2008) FT-IR, FT-Raman spectra and quantum chemical calculations of 3, 4-dimethoxyaniline. Spectrochim Acta A Mol Biomol Spectrosc 70(1):50-59. https://doi.org/10.1016/j.saa.2007.07.026
22. Coruh A, Yilmaz F, Sengez B, Kurt M, Cinar M, Karabacak M (2011) Synthesis, molecular conformation, vibrational, electronic transition, and chemical shift assignments of 4-(thiophene-3-ylmethoxy) phthalonitrile: A combined experimental and theoretical analysis. Struct Chem 22:45-56. https://doi.org/10.1007/s11224-010-9694-7
23. Meng Z, Carper WR (2002) GIAO NMR Calculation for Atrazine and Atrazine Dimers: Comparison of Theoretical and Experimenteal 1H and 13C Chemical Shifts. J Mol Struct (Theochem) 588:45-53. https://doi.org/10.1016/S0166-1280(02)00116-1
24. Sebag AB, Forsyth AD, Plante MA (2001) Conformation and configuration of tertiary amines via GIAO-derived 13C NMR chemical shifts and a multiple independent variable regression analysis. J Org Chem 66(24):7967-7973. https://doi.org/10.1021/jo001720r
25. Ditchfield R (1972) Molecular orbital theory of magnetic shielding and magnetic susceptibility. J Chem Phys 56:5688-5691. https://doi.org/10.1063/1.1677088
26. Wolinski K, Hinton JF, Pulay P (1990) Efficient implementation of the gauge-independent atomic orbital method for NMR chemical shift calculations. J Am Chem Soc 112:8251-8260. https://doi.org/10.1021/ja00179a005
27. Cimino P, Gomez-Paloma L, Duca D, Riccio R, Bifulco G (2004) Comparison of different theory models and basis sets in the calculation of 13C NMR chemical shifts of natural products. MRC 42(S1):S26-S33. https://doi.org/10.1002/mrc.1410
28. Marques MA, Gross EK (2004) Time-dependent density functional theory. Annu Rev Phys Chem 55:427-455. https://doi.org/10.1146/annurev.physchem.55.091602.094449
29. Zhao W, Bian W (2008) Investigation of the structures and electronic spectra of two coumarins with heterocyclic substituents through TD-DFT calculations. J Mol Struct (Theochem) 859:73-78. https://doi.org/10.1016/j.theochem.2008.03.004
30. Casida ME (2009) Time-dependent density-functional theory for molecules and molecular solids. J Mol Struct (Theochem) 914:3-18. https://doi.org/10.1016/j.theochem.2009.08.018

31. Runge E, Gross EK (1984) Density-functional theory for time-dependent systems. Phys Rev Lett 52:997. https://doi.org/10.1103/PhysRevLett.52.997
32. Alghamdi SK, Abbas F, Hussein RK, Alhamzani AG, El-Shamy NT (2023) Spectroscopic characterization (IR, UV-Vis), and HOMO-LUMO, MEP, NLO, NBO Analysis and the Antifungal Activity for 4- Bromo-N-(2-nitrophenyl) benzamide; Using DFT Modeling and In silico Molecular Docking. J Mol Struct 1271:134001. https://doi.org/10.1016/j.molstruc.2022.134001
33. Alguno AC, Chung WC, Bantaculo RV, Vequizo RM, Miyata H, Ignacio EW, Bacala AM (2001) Ab initio and density functional studies of polythiophene energy band gap. NTJ 2(9):215-218.
34. Govindarajan M, Karabacak M, Periandy S, Tanuja D (2012) Spectroscopic (FT-IR, FT-Raman, UV and NMR) investigation and NLO, HOMO–LUMO, nbo analysis of organic 2, 4, 5-trichloroaniline. SAA 97:231-245. https://doi.org/10.1016/j.saa.2012.06.014
35. Soliva R, Orozco M, Luque FJ (1997) Suitability of density functional methods for calculation of electrostatic properties. J Comput Chem 18(8):980-991. https://doi.org/10.1002/(SICI)1096-987X(199706)18:8<980::AID-JCC2>3.0.CO;2-M.
36. Drissi M, Benhalima N, Megrouss Y, Rachida R, Chouaih A, Hamzaoui F (2015) Theoretical and experimental electrostatic potential around the m-nitrophenol molecule. Molecules 20(3):4042-4054. https://doi.org/10.3390/molecules20034042
37. Rocha M, Di Santo A, Arias JM, Gil DM, Altabef AB (2015) Ab-initio and DFT calculations on molecular structure, NBO, HOMO–LUMO study and a new vibrational analysis of 4-(Dimethylamino) Benzaldehyde. Spectrochim Acta A Mol Biomol Spectrosc 136:635-643. http://dx.doi.org/10.1016/j.saa.2014.09.077
38. Sudhakar C, Saravanabhavan M, Ramesh KS, Badavath VN, Chandrasekar S, Babu B, Sekar M (2022) Pharmacological and quantum chemical studies of 2-aminobenzo [d] thiazol-3-ium. Results Chem 4:100442. https://doi.org/10.1016/j.rechem.2022.100442
39. Parr RG, Szentpály LV, Liu S (1999) Electrophilicity Index. J Am Chem Soc 121:1922-1924. http://doi.org/10.1021/JA983494X

Figures

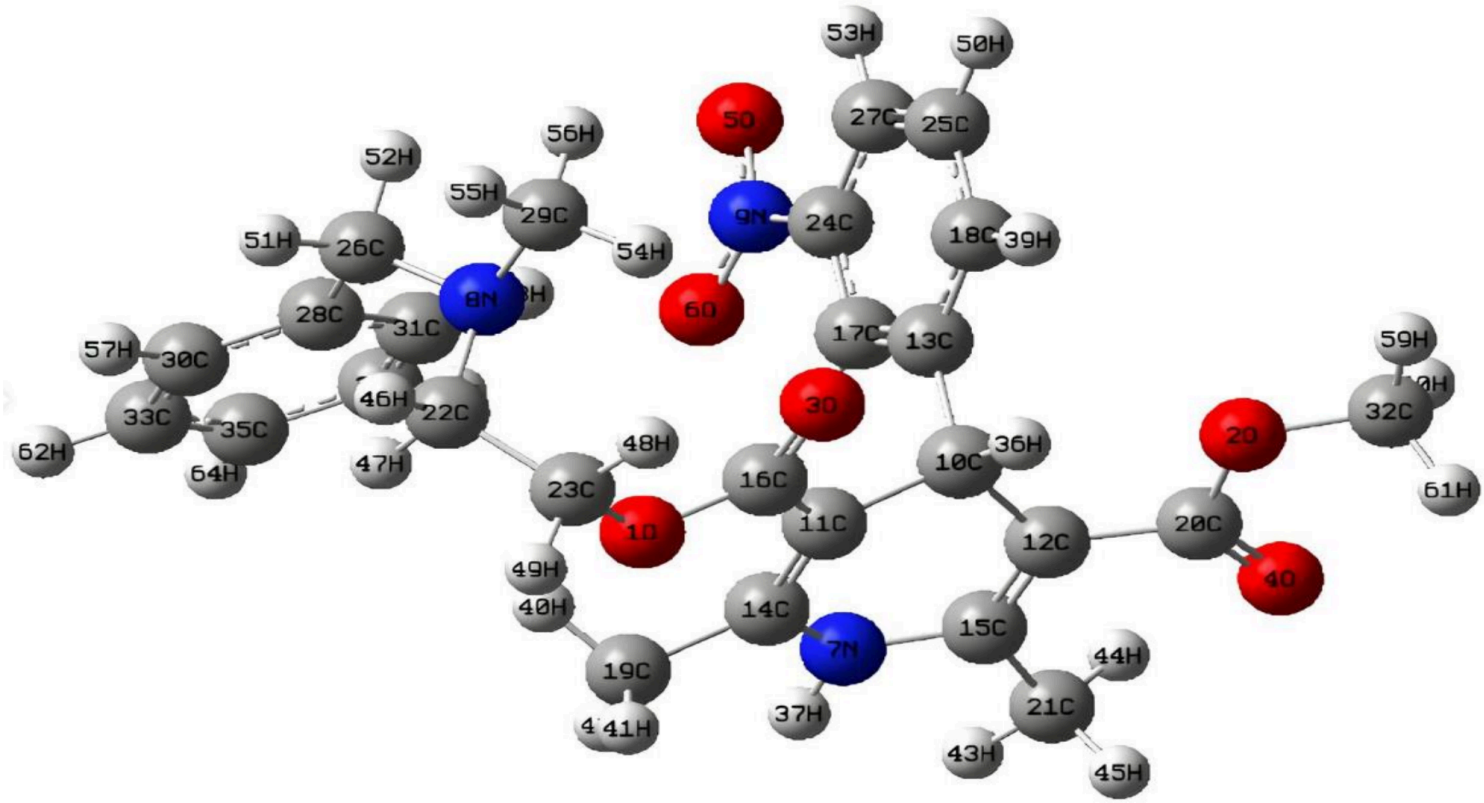

Fig. 1 Optimized Equilibrium Structure of Nicardipine (E = -1624.192; Hartree = -444196.543 eV) Obtained by B3LYP/6311++G(d,p).

Figure 1

See image above for figure legend

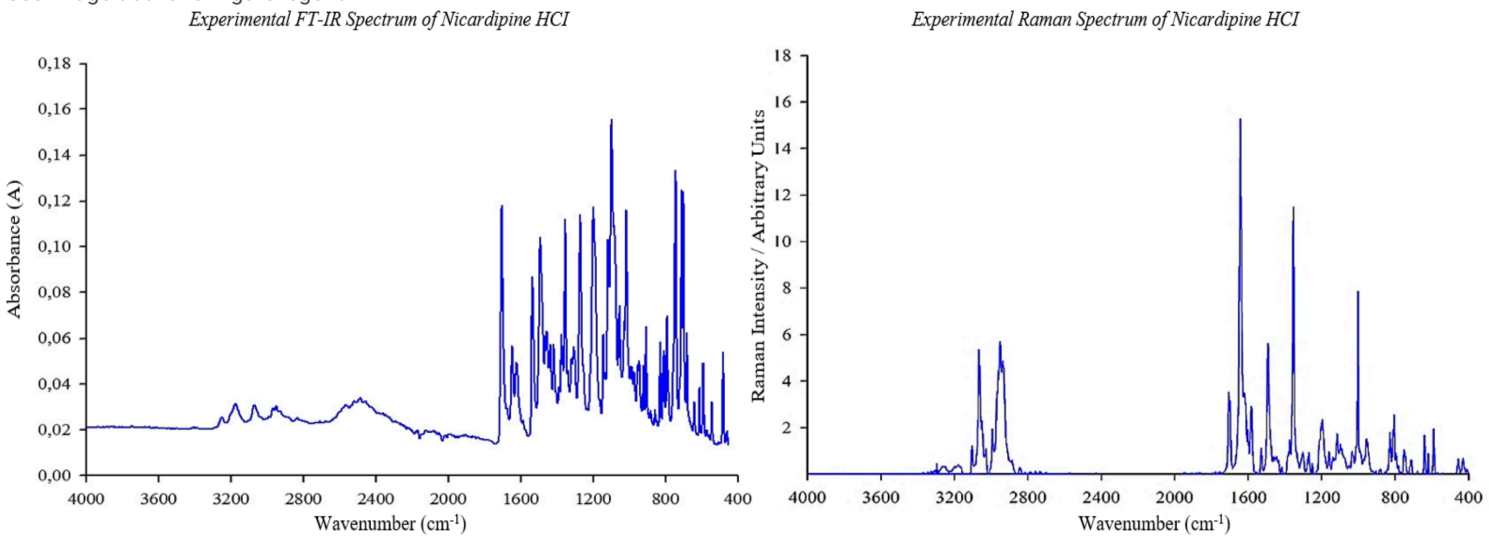

Fig. 2 Experimentally recorded FT-IR (left) and Raman (right) spectra of Nicardipine Hydrochloride

Figure 2

See image above for figure legend

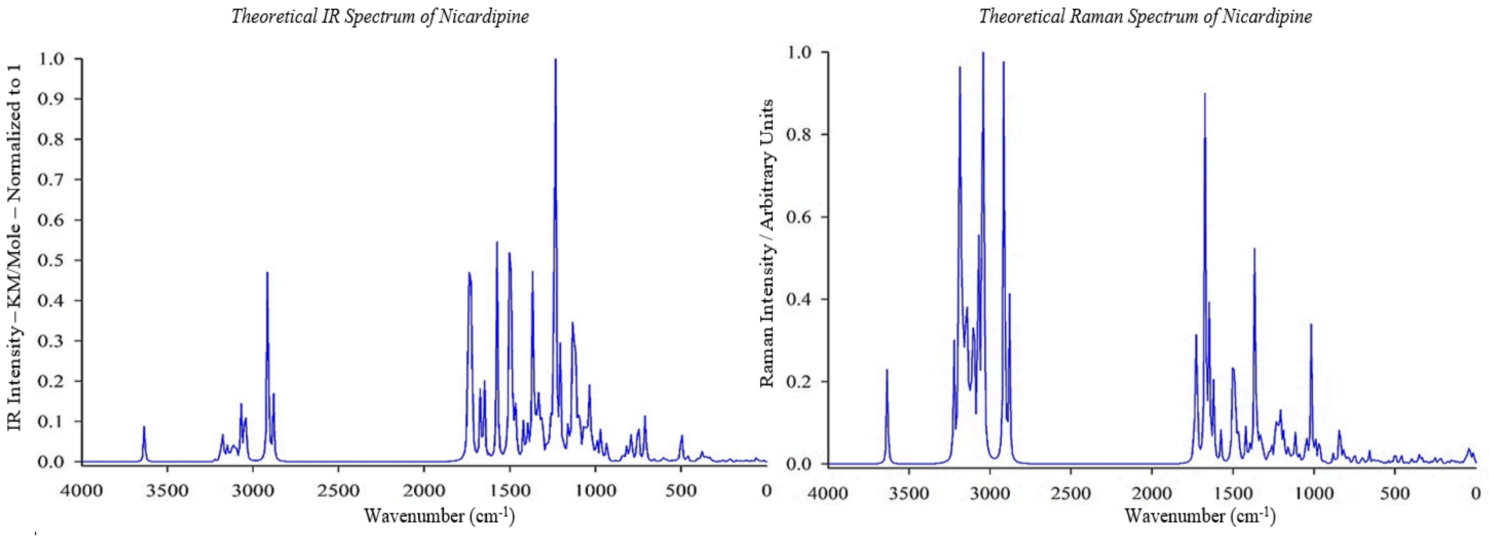

Fig. 3 Theoretically (B3LYP/6-311++G(d,p)) Obtained IR (left) and Raman (right) Spectra of Nicardipine

Figure 3

See image above for figure legend

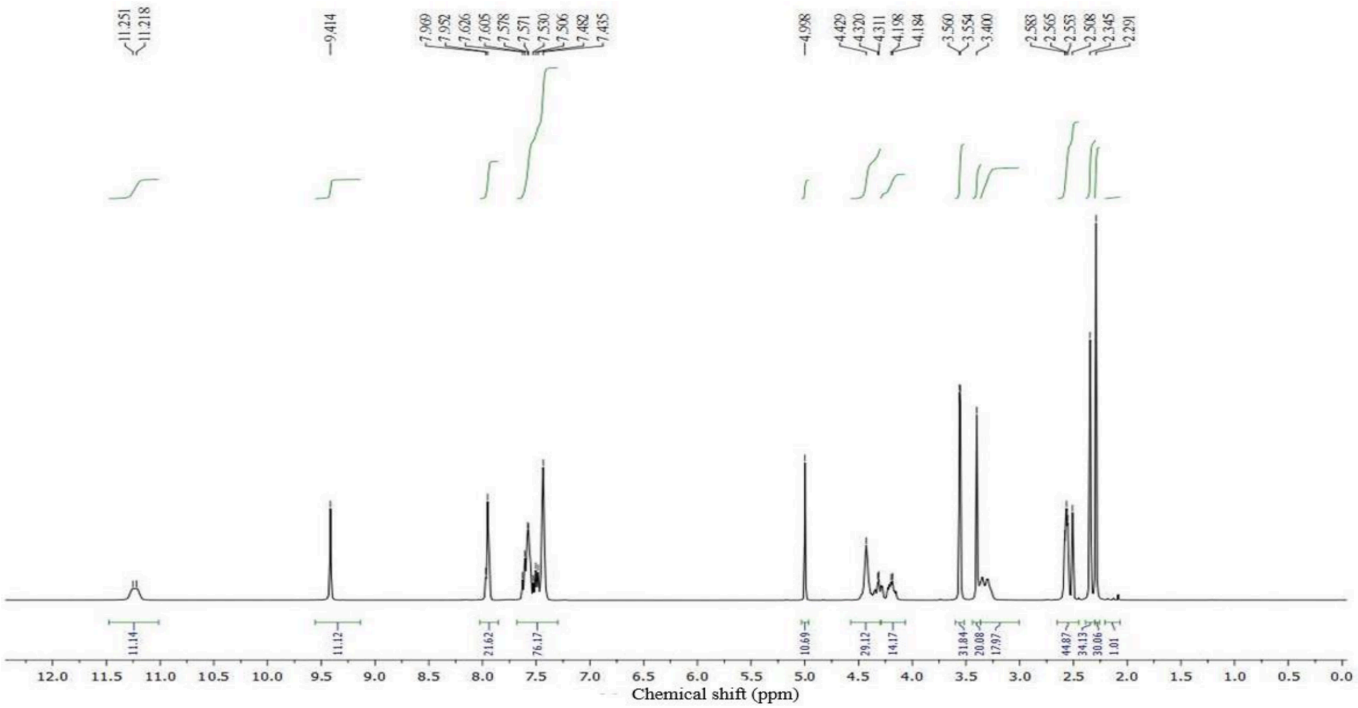

Fig. 4a Experimentally recorded ^{1}H NMR Spectrum of Nicardipine Hydrochloride

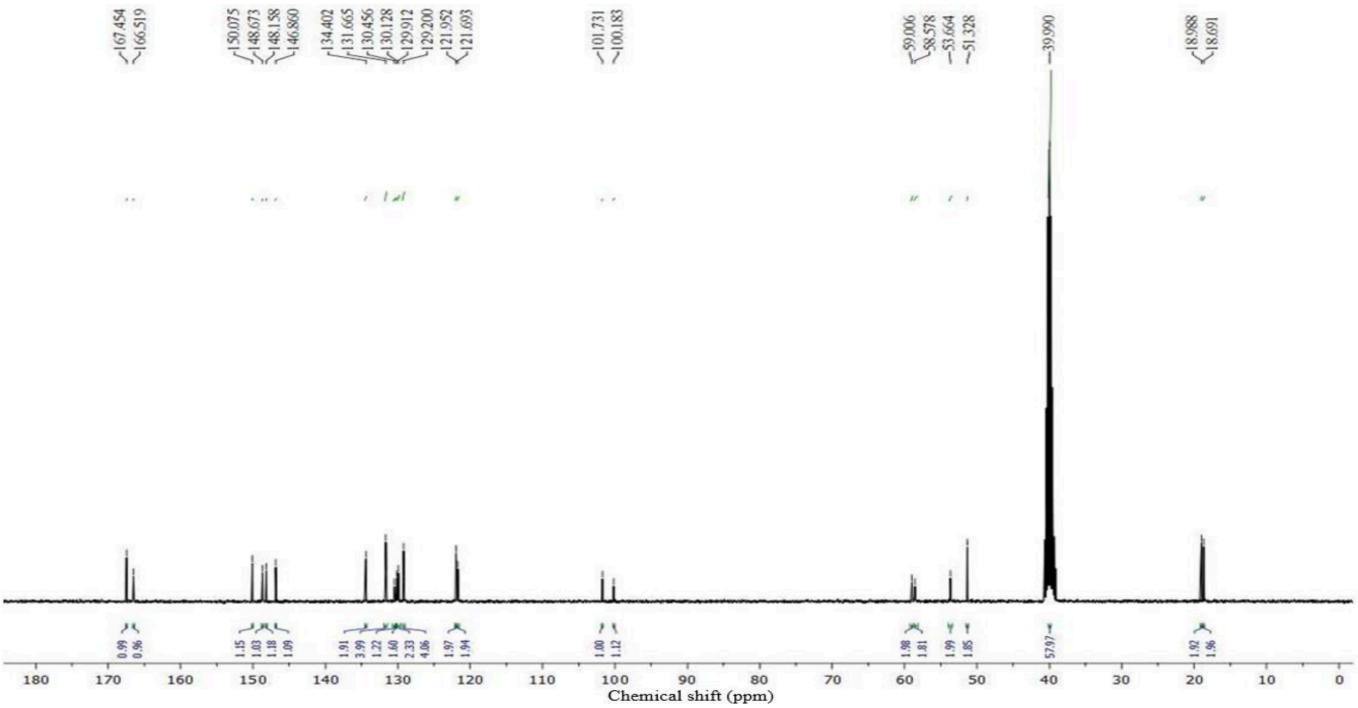

Fig. 4b Experimentally Recorded ^{13}C NMR Spectrum of Nicardipine Hydrochloride

Figure 4

See image above for figure legend

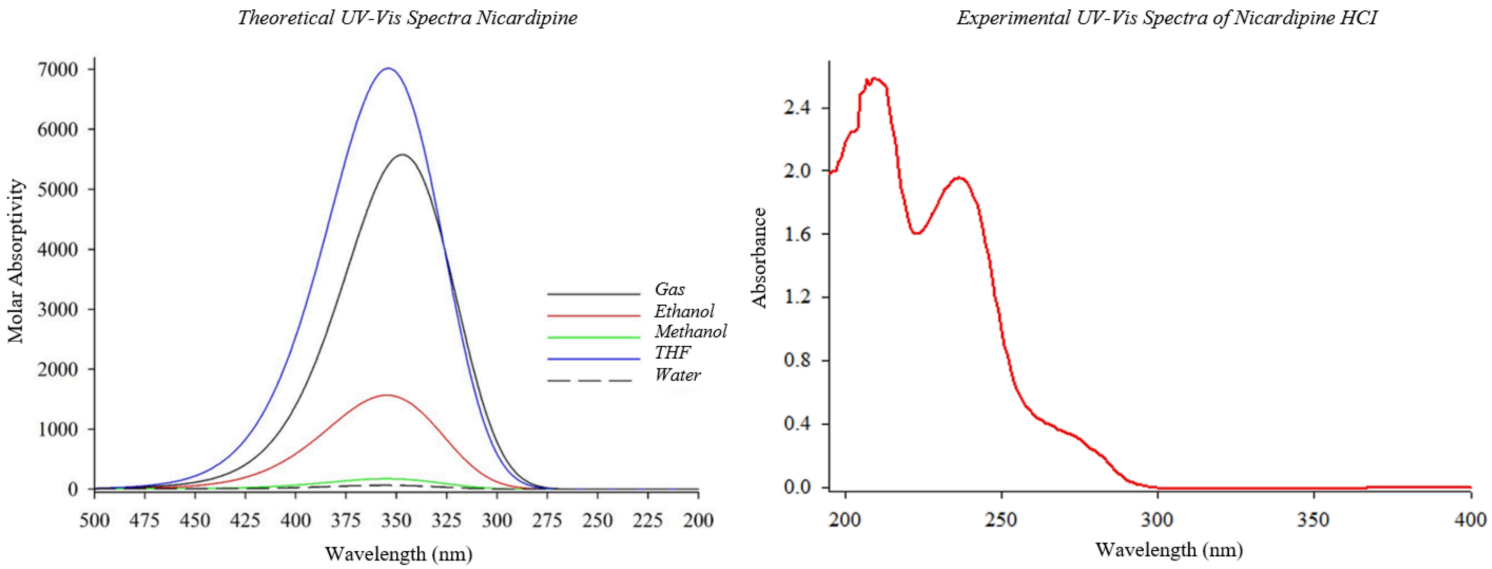

Fig. 5 Theoretical (Left) and Experimental (Right) UV-Vis Spectra of Nicardipine in Vacuum and Solvent

Figure 5

See image above for figure legend

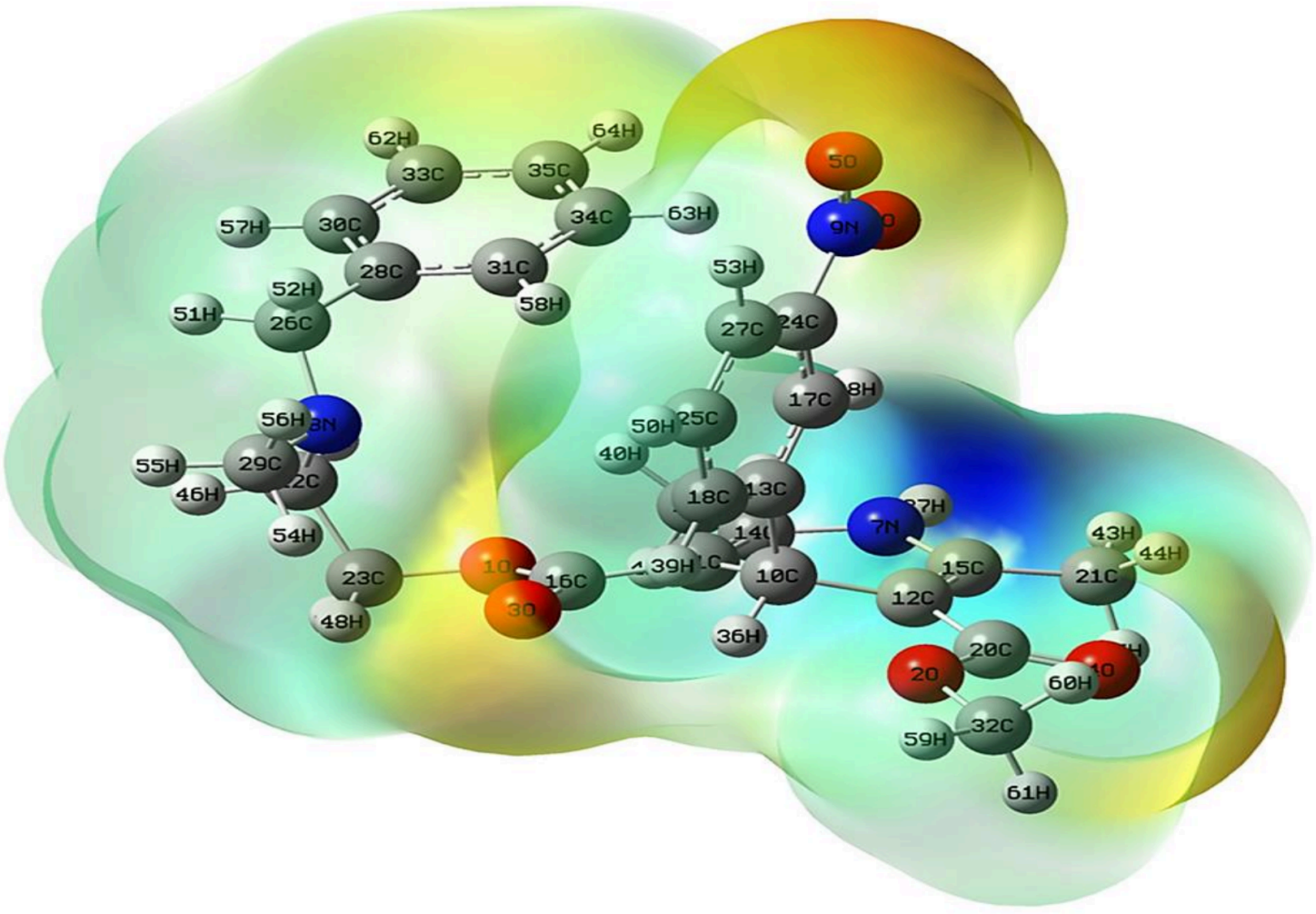

Fig. 6 The Molecular Electronic Potential Surfaces (MEPS) of Nicardipine

Figure 6

See image above for figure legend

Supplementary Files

This is a list of supplementary files associated with this preprint. Click to download.

- SupplementaryInformation.docx